JACS
JOURNAL OF THE AMERICAN CHEMICAL SOCIETY

Article

pubs.acs.org/JACS

Weakly Coupled Biologically Relevant $Cu^{II}_2(\mu\text{-}\eta^1\text{:}\eta^1\text{-}O_2)$ *cis*-Peroxo Adduct that Binds Side-On to Additional Metal Ions

Kristian E. Dalle, Tim Gruene, Sebastian Dechert, Serhiy Demeshko, and Franc Meyer*

Institut für Anorganische Chemie, Georg-August-Universität Göttingen, Tamannstrasse 4, 37077 Göttingen, Germany

Supporting Information

ABSTRACT: The ability of many copper metalloenzymes to activate O_2 and transfer it to organic substrates has motivated extensive attention in the literature. Investigations focusing on synthetic analogues have provided a detailed understanding of the structures of potential intermediates, thereby helping to guide mechanistic studies. We report herein a crystallographically characterized synthetic $Cu^{II}_2(\mu\text{-}\eta^1\text{:}\eta^1\text{-}O_2)$ complex exhibiting *cis*-peroxo bonding geometry, known in iron chemistry but previously unobserved for copper. Detailed investigation by UV−vis, resonance Raman, and infrared spectroscopies provides evidence for a significantly diminished copper−oxygen interaction ($\varepsilon \approx 3000\ M^{-1}\ cm^{-1}$, $\nu_{Cu-O} = 437\ cm^{-1}$, $\nu_{O-O} = 799\ cm^{-1}$) relative to those in known 'coupled' Cu_2O_2 species, consistent with magnetic measurements which show that the peroxide mediates only weak antiferromagnetic coupling ($-2J = 144\ cm^{-1}$). These characteristics are comparable with those of a computationally predicted transition state for O_2 binding to type 3 copper centers, providing experimental evidence for the proposed mechanism of O_2 activation and supporting the biological relevance of the $Cu^{II}_2(\mu\text{-}\eta^1\text{:}\eta^1\text{-}O_2)$ *cis*-species. The peroxide bonding arrangement also allows binding of sodium cations, observed both in the solid state and in solution. Binding induces changes on an electronic level, as monitored by UV−vis spectroscopy ($K_a = 1700\ M^{-1}$), reminiscent of redox-inactive metal binding by iron−oxygen species. The results presented highlight the analogous chemistry these reactive oxygen species undergo, with respect to both their mechanism of formation, and the molecular interactions in which they participate.

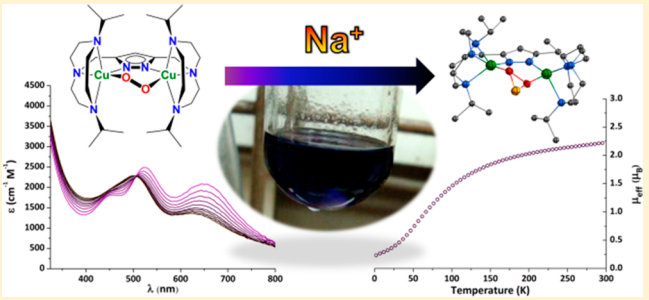

INTRODUCTION

Activation of kinetically inert dioxygen in metalloenzyme active sites can occur at dinuclear centers, such as those found in the type 3 (T3) copper proteins hemocyanin (Hc) and tyrosinase (Tyr).[1,2] Understanding how these proteins accomplish this is of great fundamental interest, and they additionally serve as archetypes for achieving selective oxygenation and oxidation reactions with bioinspired catalysts.[3] Synthetic analogues have granted structural insights such as elucidation of the oxygen-binding mode in Hc[4] and, through reactivity correlations, form the basis of the ongoing debate over the oxygenation mechanism in Tyr.[1,5] Various oligocopper−oxygen adducts have been characterized upon reaction of copper(I) model complexes with dioxygen (Figure 1A), including several not observed in the parental enzymes.[6−9] Despite the *trans*-$Cu^{II}_2(\mu\text{-}\eta^1\text{:}\eta^1\text{-}O_2)$ (^{T}P) being the first of these Cu_2O_2 species to be structurally characterized,[10] there appears to be a distinct lack in the literature of the corresponding *cis*-structure (^{C}P). Although the ^{T}P species are not considered to be biologically relevant, the ^{C}P configuration is thought to play a significant role in facilitating O_2 binding in Hc.[11] Analogous nonheme diiron species are also established intermediates in the related O_2 activation achieved by enzymes such as soluble methane monooxygenase (sMMO) and ribonucleotide reductase (RNR).[12,13]

Bonding between copper and peroxide in Cu_2O_2 species has been extensively investigated by Solomon and co-workers, owing to relevance to T3 "coupled" dinuclear copper centers.[5,11,14−16] The term "coupled" here refers to the strong antiferromagnetic coupling between the copper(II) ions in the active sites of these enyzmes. This magnetic coupling in both the natural (^{S}P) and model (^{S}P and ^{T}P) systems results from the planar nature of their Cu_2O_2 cores, which maximizes the interaction between the symmetric combination of copper(II) magnetic orbitals and one of the two O_2^{2-} π^* HOMOs (Figure 1C).[5,11] The extent of this interaction is reflected in the magnitude of antiferromagnetic coupling and the intensity of the CT transitions.[15−17] It is also the major contributor to Cu−O bonding, and helps dictate the O−O bond strength as it transfers electron density from peroxide π^* to copper d orbitals (a second interaction complements this in ^{S}P species).[14−16]

A DFT study has also elucidated an elegant mechanism for the spin forbidden activation of dioxygen by T3 centers.[11] In the initial stages of O_2 binding, a ^{C}P species has been identified with a Cu−OO−Cu torsion angle which allows the two perpendicular O_2 π^* orbitals to simultaneously interact with the bimetallic site, each with a different copper(I) ion. This allows

Received: March 14, 2014
Published: April 25, 2014

   dx.doi.org/10.1021/ja5025047 | J. Am. Chem. Soc. 2014, 136, 7428−7434

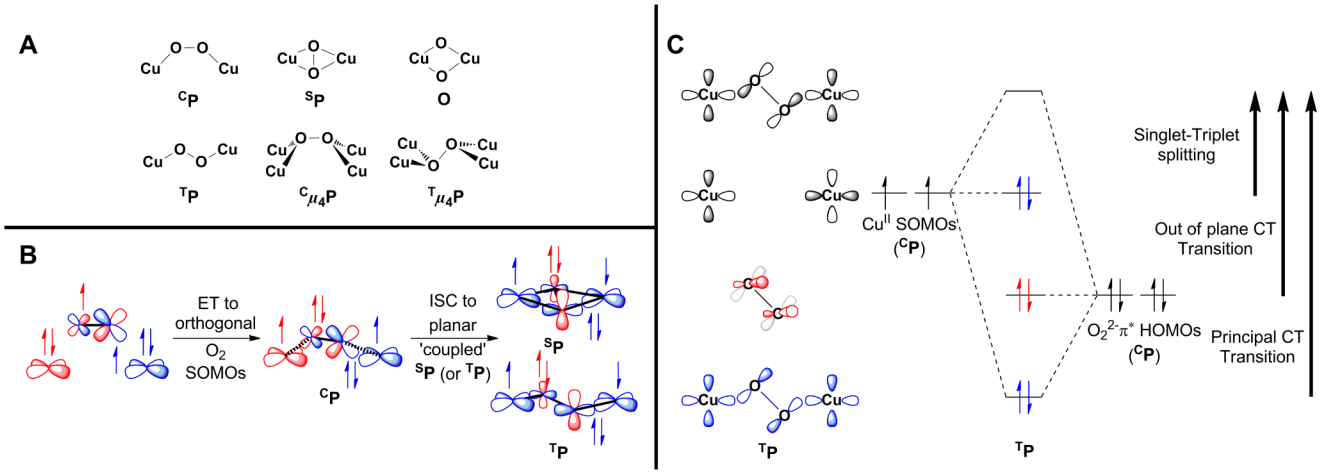

Figure 1. (A) Selection of structurally characterized Cu_n-O_2 adducts. The ^{C}P type is reported here for the first time. (B) Mechanism for O_2 binding by Hc (and Tyr), which leads to a singlet state ^{S}P core (or ^{T}P in synthetic models). The intermediate structure is a ^{C}P type Cu_2O_2 adduct.[11] (C) Electronic structure of ^{T}P species, with MOs on the left. On the right are the associated spectroscopic features, which are proportional to the extent of copper(II)-peroxide bonding.[5,16]

synchronous transfer of two electrons of the same spin to orthogonal dioxygen orbitals, reducing O_2 to O_2^{2-} and delocalizing the unpaired spins to the distal copper(II) ions (Figure 1B). Progression to the planar Cu_2O_2 core then establishes a superexchange pathway capable of overcoming spin−spin repulsion and enabling intersystem crossing (ISC) to the "coupled" singlet state. A ^{C}P structure with an appropriate Cu−OO−Cu torsion angle should thus offer insight into the early stages of T3-mediated O_2 activation.

Some time ago, the $^{T}\mu$-$_4$P structure shown in Figure 1A was reported after exposure of a pyrazolate-bridged dinuclear copper(I) complex to aerial dioxygen.[18] While the mechanistic details are still unclear, a plausible reaction pathway would proceed through a ^{C}P intermediate, followed by subsequent "trapping" with a second dinuclear copper complex. As a strategy for hindering this dimerization, and thus isolating the elusive ^{C}P species, we now employed a pyrazole-triazacyclononane hybrid ligand scaffold ($\mathbf{HL}^{\mathbf{PzTACN}}$)[19,20] with additional donor atoms and steric bulk. The corresponding dinuclear copper(I) complex (**1**) showed formation of a thermally labile dioxygen adduct, even at ambient temperatures. We thus herein report the first known example of a biologically relevant ^{C}P type $Cu^{II}_2(\mu\text{-}\eta^1\text{:}\eta^1\text{-}O_2)$ species (**2**), possessing a unique *cis*-peroxo bonding arrangement which mediates weak magnetic coupling and enables side-on binding to additional metal ions.

RESULTS AND DISCUSSION

In situ generation of the dinuclear copper(I) complex (**1**) was achieved by deprotonation of $\mathbf{HL}^{\mathbf{PzTACN}}$ with sodium *tert*-butoxide, followed by addition of 2 equiv of $[Cu^{I}(CH_3CN)_4]$-OTf (OTf = $CF_3SO_3^-$)[21] in propionitrile (EtCN), as confirmed by NMR spectroscopy and ESI-MS [see the Supporting Information (SI), section 1]. Exposure to gaseous O_2 directly, or after exchanging the solvent to acetone (Me_2CO), resulted in thermally labile, intensely purple colored solutions, which even persisted for some minutes at room temperature. UV−vis spectroscopy at −30 °C revealed a principal band at 500 nm ($\varepsilon \approx 3000$ M^{-1} cm^{-1}), and a broad shoulder at 630 nm, qualitatively similar to those of ^{T}P species.[6,22−24] Further evidence confirming the formation of a copper peroxide species (**2**, Figure 2A) was obtained by resonance Raman (rR)

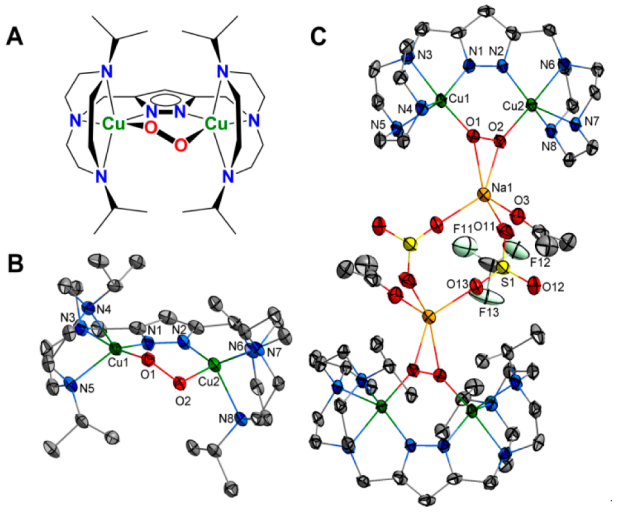

Figure 2. (A) Pictorial representation of B; (B) dicopper complex unit of **2** showing the unique peroxide binding mode and torsion angle; (C) full symmetric dimer displaying the side-on binding to the sodium cation, allowing for bridging by NaOTf (selected *iso*-propyl and $-CF_3$ groups omitted for clarity). Ellipsoids are drawn at 30% probability.

spectroscopy with a laser excitation of 633 nm (Figure 3A). Cooled solutions (−30 °C) of **2** showed two oxygen isotope sensitive features at 799 and 437 cm^{-1} ($\Delta^{16}O_2-^{18}O_2$ = 45 and 19 cm^{-1}, respectively; exact determination is complicated by Fermi resonance and overlap with a solvent signal; the average shift of the two $^{16}O_2$ bands after subtraction of the solvent signal is reported; see SI section 4 for more detail), characteristic of an end-on peroxide moiety bridging two copper(II) ions, albeit with a significantly lower Cu−O stretching frequency.[6,23−26] Binding of O_2 is irreversible (no backward reaction observed upon applying vacuum or purging with argon, with and without warming) and was found to proceed in 80−90% yield by monitoring O_2 uptake with a Clark electrode (Figure S3).

Unambiguous determination of the peroxide binding mode was provided by X-ray diffraction (see SI Section 3 for details).[27−32] The molecular structure, shown in Figure 2, represents the first crystallographically characterized end-on

dx.doi.org/10.1021/ja5025047 | J. Am. Chem. Soc. 2014, 136, 7428−7434

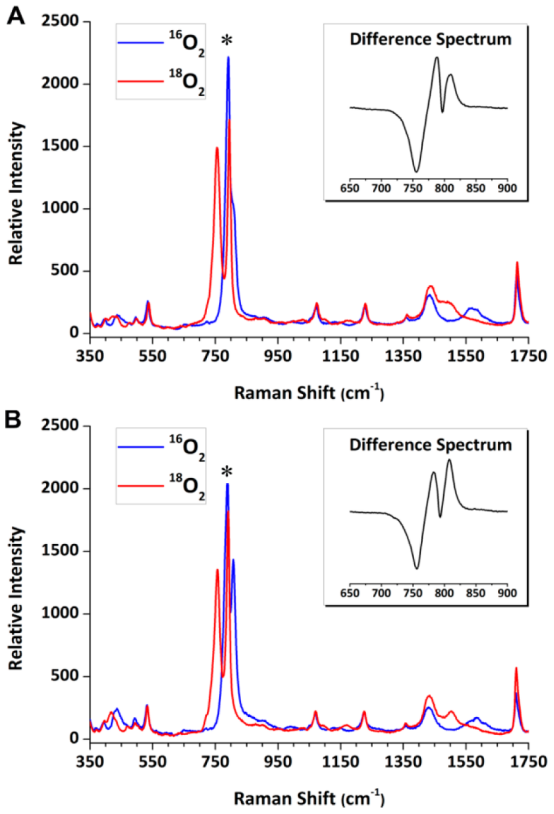

Figure 3. rR spectra of (A) **2** and (B) **2**$^{-Na}$ in Me_2CO at −30 °C. The doublet in the $^{16}O_2$ spectra (blue) disappears upon reaction with $^{18}O_2$ (red) consistent with a Fermi Resonance,[42,43] which has previously been observed in these systems.[25,26] A solvent band (*) overlaps with the $^{16}O_2$ O−O stretches in both cases. An overtone of this O−O vibration can be observed in both the $^{16}O_2$ and $^{18}O_2$ spectra.

$Cu^{II}_2(\mu\text{-}\eta^1\text{:}\eta^1\text{-}O_2)$ peroxide species with a *cis*-geometry (^{C}P, Figure 1A), in contrast with the four known structurally authenticated examples of the *trans*-(^{T}P) configuration (Table 1).[10,26,33,35] The complex cation is a dimeric structure, bridged by co-crystallized NaOTf, with a crystallographically imposed inversion center. The coordination spheres around each copper atom lie close to the midpoint between the idealized square pyramidal and trigonal bipyramidal geometries, with tau factors (τ)[36] of 0.59 and 0.57 for Cu1 and Cu2, respectively. Copper−ligand bond lengths are significantly shorter for the peroxide and pyrazolate anionic bridging donors (1.899−1.916 Å) than those of the neutral side arm nitrogen atoms (2.134−2.194 Å). Although these metric parameters all fall within the range already observed for ^{T}P species, it should be noted that the peroxide ligand bond length (O−O = 1.498 Å) is at the upper limit of those known. In contrast, the intermetallic distance in **2** (Cu···Cu = 3.797 Å) is substantially (>0.5 Å) shorter than in all ^{T}P species, and this unique situation imposes a significant torsion angle (φ) upon the bridging peroxide ligand (Cu−OO−Cu = 65.2°), the implications of which are discussed below.

A remarkable structural feature of **2** is the close contact of the peroxide moiety with the sodium cation. The Na−O distances in **2** (2.296/2.302 Å) are shorter than those of the side-on bound sodium cations in anhydrous ionic Na_2O_2 (2.322/2.404 Å).[37] Although few in number, other known metal-O_2^{2-} complexes (metal = Ti,[38] Ga,[39] Mo,[40] Pu[41]) exhibiting side-on peroxide−sodium interactions have an average Na−O distance of 2.404 Å (range: 2.251−2.604 Å). While direct comparison is difficult owing to differing sodium coligands and co-ordination numbers, the Na−O interaction in **2** suggests that the peroxide moiety retains a significant amount of negative charge. **2** was found to be surprisingly stable in the solid state (heating to 60 °C or applying vacuum overnight caused no significant decomposition as monitored by rR). This may be tentatively attributed to shielding of the peroxide in the solid state provided by the co-crystallized NaOTf, analogous to that of the $[B(C_6H_5)_4]^-$ counteranion recently observed by Schindler and co-workers.[26] Furthermore, interaction of redox-inactive Lewis acidic metal cations with transition metal−oxygen adducts, such as calcium, zinc, and scandium binding to high-valent manganese- or iron-oxo species, has been shown to significantly influence the reactivity of the oxo species, and is currently a topic of considerable interest in the literature.[44−49] Very recently, such modulation of reactivity was also demonstrated in a mononuclear $Fe^{III}(\eta^2\text{-}O_2)$ peroxo species.[50] Thus, NaOTf association in solution was further investigated.

Sodium Binding in Solution. Sodium-free dinuclear copper(I) complex (**1**$^{-Na}$) was prepared through the use of copper *tert*-butoxide (SI, section 1).[51] Initial insight was provided by comparing solution state rR spectra for **2** and **2**$^{-Na}$, which revealed slight changes in the O−O stretching frequency (<5 cm^{-1} toward higher frequency, Figure 3) in the absence of sodium cations. While exposure to gaseous O_2 again formed intensely colored purple solutions (**2**$^{-Na}$), the resulting UV−vis spectra were found to subtly but significantly differ

Table 1. Metric and Spectroscopic Parameters of Crystallographically Characterized $Cu^{II}_2(\mu\text{-}\eta^1\text{:}\eta^1\text{-}O_2)$ Complexes

ligand[a]	species	Cu−O (Å)	Cu···Cu (Å)	O−O (Å)	∠Cu−OO−Cu (deg)	ν_{O-O} (cm^{-1})	ν_{Cu-O} (cm^{-1})	λ_{max} (nm)	ε (M^{-1} cm^{-1})	ref.
TMPA	^{T}P	1.852	4.359	1.432	180.0	826[b]	561[b]	525	11 300	10,16
						832[c]	554[c]			
Bz_3tren	^{T}P	1.867	4.476	1.450	180.0	839/829[b]	556/539[b]	518	14 900	33
						-	-			
Me_6tren	^{T}P	1.907	4.590	1.368	180.0	825[b]	-	552	13 500	26,34
						820/809[c]	585/541[c]			
Tet b	^{T}P	1.939/1.923	4.566	1.495	143.7	-	-	550	-	35
						828/811[c]	-			
L^{PzTACN}	^{C}P	1.899/1.916	3.797	1.498	65.2	799[b]	437[b]	500	3000	This work
						788[c]	448[c]			

[a]TMPA = tris(pyridin-2-ylmethyl)amine, Bz_3tren = tris[2-(benzylamino)ethyl]amine, Me_6tren = tris[2-(dimethylamino)ethyl]amine, and Tet *b* = rac-5,5,7,12,12,14-hexamethyl-1,4,8,11-tetraazacyclotetradecane. All listed ^{T}P species contain two ligands per dimeric Cu_2O_2 unit. [b]In solution. [c]Solid state.

dx.doi.org/10.1021/ja5025047 | J. Am. Chem. Soc. 2014, 136, 7428−7434

from that of **2**; the absorption bands appear to undergo a red shift with the shoulder simultaneously gaining intensity. Further investigation revealed that the above-reported spectra for **2** are observed only for relatively concentrated ($\geq 5 \times 10^{-3}$ M) solutions, whereas at lower concentrations ($\leq 2.5 \times 10^{-4}$ M) they are indistinguishable from those of $\mathbf{2}^{\text{-Na}}$. Introducing additional sodium ions (NaOTf or $NaBPh_4$) to dilute solutions of **2** caused a reversal of this trend (Figure 4), the extent of

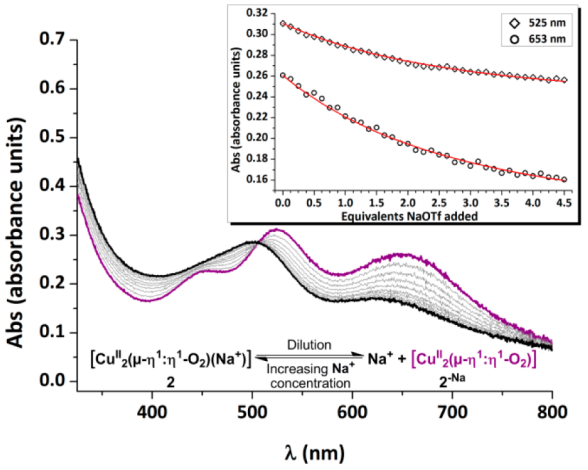

Figure 4. UV−vis spectra of NaOTf titration of $\mathbf{2}^{\text{-Na}}$ at −30 °C. The isosbestic point is at 507 nm. The inset shows the changes in absorbance as a function of NaOTf added. The red curves in the inset show the best fit used to derive the binding constant (see SI Section 5).

which correlated with the amount of excess sodium salt added, up to the maximum value of concentrated solutions of **2**. Concentrated solutions of **2** are also in very good agreement with the solid state reflectance spectrum of **2** (SI, Figure S12). These results indicate that sodium ions bind to the peroxide moiety in solution in a concentration dependent equilibrium. An association constant (K_a) of 1700 (±10%) M^{-1} was determined by correlating changes in absorbance with introduction of sodium ions (Figure 4 inset, see SI Section 5 for more details).[52]

In contrast to the above results, adding triflate anion (Bu_4NOTf) to dilute solutions of **2** caused no observable changes in the UV−vis spectra, indicating that triflate is not involved in the equilibrium. This was confirmed by ^{19}F NMR diffusion-ordered spectroscopy (DOSY) at −30 °C. Solutions of **2** in d_3-MeCN or d_6-acetone displayed diffusion coefficients identical to that of Bu_4NOTf, indicating complete dissociation of the triflate anions. Attempts to directly assess the change in molecular size between **2** and $\mathbf{2}^{\text{-Na}}$ were unfortunately unsuccessful, as ^1H NMR spectra at low temperature showed extremely broad (>100 Hz), paramagnetically shifted (δ = 5−54 ppm) resonances which were not useful for further analysis.

Magnetism. The high stability of **2** in the solid state allowed further investigation of the observed paramagnetism by SQUID magnetometry. The magnetic susceptibility data (Figure 5A) indicate an $S = 0$ ground state with a singlet−triplet splitting of $-2J = 144$ cm^{-1} ($-2JS_1S_2$ model; see SI section 6). This value is significantly smaller than those experimentally determined as $-2J \geq 600$ cm^{-1} for the essentially diamagnetic ^{T}P species $[(TMPA)_2Cu_2(O_2)]^{2+}$ (TMPA = see Table 1)[53] and ^{S}P species oxyhemocyanin

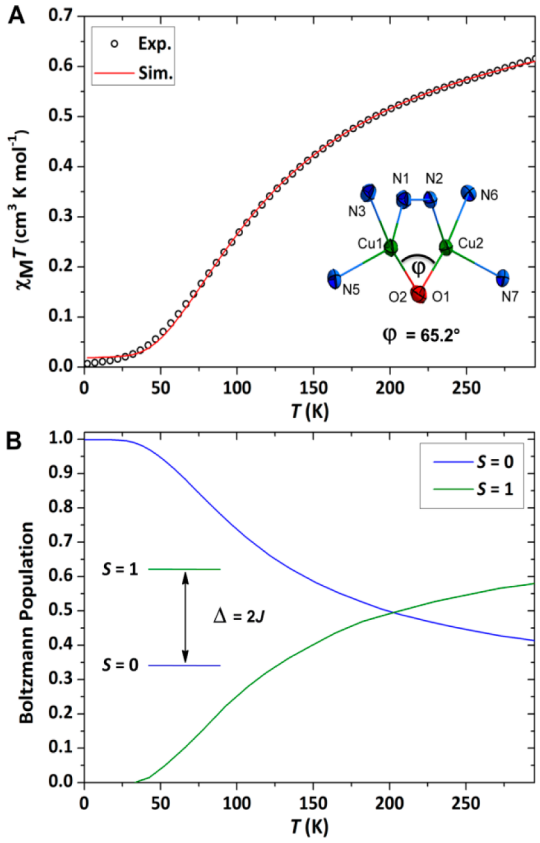

Figure 5. Magnetic properties of **2**. (A) Temperature dependence of the $\chi_M T$ product for compound **2** between 295 and 2 K. The red line shows the best fit curve. The inset shows the torsion angle (φ) looking down the O1−O2 bond (N4 and N8 omitted for clarity), which in part gives rise to the weak coupling. (B) Boltzmann distribution simulated using $-2J = 144$ cm^{-1} and showing the thermal population of the energetically higher $S = 1$ spin state (see SI section 6 for details).

(oxyHc)[54] and $[(N4)Cu_2(O_2)]^{2+}$ (N4 = *N,N,N′,N′*-tetrakis(2-(pyridin-2-yl)ethyl)butane-1,4-diamine).[53]

When present as the only pathway between two Cu(II) ions the pyrazolate unit mediates relatively weak to moderate ($-2J$ = 26 to 70 cm^{-1}) antiferromagnetic coupling.[55−57] The superexchange contribution from the peroxide bridge in **2** is thus extremely diminished when compared with that of ^{T}P and ^{S}P species. This can be rationalized by taking into account the unique bonding situation in **2**. We have previously shown that the magnetic coupling in dinuclear copper(II) and nickel(II) complexes supported by pyrazolate-bridging ligand scaffolds strongly depends on the torsion angle along the pyrazolate N−N bond[58,59] and along the exogenous ligand. With respect to the latter, a ($\mu_{1,3}$-azido)(μ-pyrazolato)dinickel(II) complex was found to undergo reversible thermally induced conformational switching in the solid state, exhibiting a pronounced change in antiferromagnetic coupling ($-2J$ = 162 cm^{-1} vs 48 cm^{-1}) between the two conformers as a result of the differing $\mu_{1,3}$-azido torsion angles (Ni-NNN-Ni = 4.3° vs −46.6°, respectively).[60] In the case of torsion angles approaching 90°, only orthogonal orbitals of the bridging ligand will be able to interact with the metal-based SOMOs, leading to ferromagnetic coupling.[58,59] The Cu−OO−Cu torsion of 65.2° in **2** is thus in accordance with relatively weak antiferromagnetic coupling.

Biological Relevance. Taken together, the data for **2** show that it indeed possesses characteristics that would be expected

dx.doi.org/10.1021/ja5025047 | J. Am. Chem. Soc. 2014, 136, 7428−7434

in an early stage of oxygen binding to T3 dicopper sites, as exemplified by comparison to the known $Cu^{II}_2(\mu\text{-}\eta^1\text{:}\eta^1\text{-}O_2)$ species. The Cu−O stretching vibration is found near 450 cm^{-1}, lower by far than any other reported. This suggests a reduced degree of covalency, further supported by the molar extinction coefficient of ∼3000 M^{-1} cm^{-1}, which indicates that the peroxide σ-donor interaction is significantly diminished.[15,17] This in turn is reflected in the O−O stretching frequency of 799 cm^{-1}, which is among the lowest reported values for $Cu^{II}_2(\mu\text{-}\eta^1\text{:}\eta^1\text{-}O_2)$ species, and is consistent with the long O−O bond length of 1.498 Å which lies at the upper limit of those known. These observations can be qualitatively explained by considering the above description of bonding developed by Solomon and co-workers.[5,16] As a result of the torsion angle in **2**, interaction between the valence peroxide and Cu orbitals is significantly reduced. This leads to a decrease in the covalency of the Cu−O bonds while at the same time hindering the O_2^{2-} π^* → Cu(II) charge transfer donation, resulting in more electron density in orbitals which are antibonding with respect to the O−O bond. In addition, overlap of a single O_2^{2-} π^* orbital with both half-filled Cu(II) orbitals is not possible. The torsion angle in **2** in fact makes interaction with orthogonal O_2^{2-} π^* orbitals much more feasible (Figure 5A inset). This attenuates the superexchange pathway and results in weak antiferromagnetic coupling relative to ^{T}P and ^{S}P species, indicating that **2** lies close to the border of the ISC event. **2** thus represents a snapshot of an intermediate in the binding of O_2 to Hc, and provides strong experimental support for the aforementioned mechanism of dioxygen activation.

Preliminary Reactivity. The bonding considerations described above suggest that the peroxide moiety in **2** should retain significant charge density, as supported by the observed interaction with sodium cations. Additionally, as evidenced by ^{1}H NMR, the weak antiferromagnetic coupling results in significant thermal population of the energetically higher S = 1 spin state, even at −30 °C (Figure 5B). Spin state is known to have a profound effect on resulting reactivity.[61,62] Indeed, warming of solutions of **2** or $\mathbf{2}^{\text{-Na}}$ in the presence of an excess of dihydroanthracene (DHA) led to formation of anthracene in ∼25% yield (per dicopper unit) by subsequent ^{1}H NMR analysis (Figure S14). Such radical-like reactivity is normally associated with high-valency species such as those with $Cu^{III}_2(\mu\text{-}O)_2$ (**O** in Figure 1A) or $Fe^{IV}(O)$ functionality.[7,8,61] However, reaction with DHA was only observed to occur upon warming to room temperature, possibly implicating a decomposition product as the active species. While these observations can be tentatively attributed to the partial radical-like nature of **2**, further investigation is needed to corroborate these findings. Efforts to establish the reactivity patterns of **2** using various reagents of differing character are ongoing, and we already have substantial experimental evidence that binding of redox-inactive Lewis acidic metal cations is not limited to sodium.

CONCLUSION

We have presented the first crystallographically characterized example of a $Cu^{II}_2(\mu\text{-}\eta^1\text{:}\eta^1\text{-}O_2)$ *cis*-peroxo species. This bonding arrangement results in properties which support the proposed mechanism for the activation of dioxygen by T3 copper proteins, and **2** may thus represent a biologically relevant transition state model. This novel structure serves to highlight the parallels between dinuclear enzymatic oxygen activation pathways in copper and iron enzymes. These similarities are further emphasized by the unusual sodium ion interaction displayed by **2**. Binding to a redox-inactive metal in solution induces changes on an electronic level; analogous behavior has been observed in synthetic manganese− and iron−oxygen adducts. Theoretical studies aimed at gaining a more quantitative description of the electronic structure, and thereby elucidating the full effects of sodium ion binding, are in progress. The results presented here serve to illustrate the common features shared by reactive oxygen species, and provide directions for further investigations into bioinspired oxygenation and oxidation catalysis. Given that the metal−metal separation in complexes with pyrazolate-derived compartmental scaffolds can be tuned via proper ligand design,[19,20,63,64] we now target a dicopper(II)-peroxo species that features an even shorter Cu···Cu distance, imposing a torsion angle of close to 90° and potentially resulting in an S = 1 ground state.

EXPERIMENTAL SECTION

Synthesis. More detailed synthetic procedures together with characterization data can be found in Section 1 of the SI. A general method was followed for preparation of all complex solutions used, whereby $\mathbf{HL}^{\text{PzTACN}}$ and NaO^{t}Bu were reacted in propionitrile (EtCN). $[Cu(MeCN)_4]OTf$ (MeCN = CH_3CN, OTf = $CF_3SO_3^-$) dissolved in EtCN was added dropwise, and after evaporation of all volatile material under reduced pressure the resulting residue was redissolved in Me_2CO or EtCN. The resulting solutions were used for all further experiments, including crystallization. The sodium-free variant of **1** was prepared analogously, with substitution of NaO^{t}Bu and 1 equiv of $[Cu(MeCN)_4]OTf$ by CuO^{t}Bu.

Oxygen Uptake. Oxygen uptake experiments were performed in a small (<5 mL) cell closed with a septum and maintained at −30 °C. A Clark-type gas phase oxygen sensor (Ox-N sensor and Oxy-meter, Unisense) was inserted through the septum into the head space of the cell. The sensor was calibrated before each experiment. A Hamilton Sample Lock syringe was thus used to add 250 μL portions of oxygen to the gas phase of the cell, containing 1 mL of dry, degassed Me_2CO. The dried cell was then filled with 1 mL of a 1×10^{-2} M solution of **1** inside the glovebox and closed with a new septum. After temperature equilibration, the sensor was inserted into the cell (very slight color change of the solution was observed) and, after waiting until the signal was stable (typically 10 min), 250 μL of O_2 was injected. Further O_2 injections were carried out after signal stabilization to check for further reaction and confirm that the cell was gastight. See SI section 2 for experimental traces.

Crystallography. Suitable crystals were obtained by slow Et_2O diffusion into an Me_2CO solution of **2** at −30 °C. Diffraction data was collected both in-house on an STOE IPDS II diffractometer and at beamline BL14.1 at the BESSY synchrotron. Two data sets have therefore been deposited with the Cambridge Crystallographic Data Centre under the reference numbers CCDC-984199 and CCDC-984213. For more details see SI section 3.

Resonance Raman Spectroscopy. Resonance Raman spectra were measured using a HORIBA Scientific LabRAM HR 800 (400−1100 nm) spectrometer with open-electrode CCD detector and a confocal pinhole with user controlled variable aperture, in combination with a free space optical microscope and a He:Ne-laser (632.8 nm). A CryoVac KONTI-Cryostat-Mikro cell with liquid N_2 cooling cryostat was used for solution measurements. 1×10^{-2} M solutions of **1** or $\mathbf{1}^{\text{-Na}}$ were injected into the cell. After allowing the temperature to equilibrate, dioxygen gas was admitted to the cell. $^{18}O_2$ samples were prepared from the same stock solutions at a Schlenk line and then directly injected into the cell. Solid state measurements were performed under air with the sample mounted on a glass slide. For more details see SI section 4.

UV−vis Measurements. Low temperature UV−vis spectra were measured with a Varian Cary 50 Bio instrument coupled to a quartz immersion probe (5 mm, Hellma Analytics). Temperature stability was

dx.doi.org/10.1021/ja5025047 | J. Am. Chem. Soc. 2014, 136, 7428−7434

qualitatively assessed using the quartz immersion probe. Temperature regulated solutions of **1** or $\mathbf{1}^{-Na}$ were exposed to gaseous dioxygen by atmosphere exchange. The sodium binding titration was conducted at −30 °C with a 2.5×10^{-4} M solution of $\mathbf{2}^{-Na}$ to which a 4.7×10^{-3} M NaOTf solution was added in 0.016 mL aliquots. Investigation into thermally induced decomposition and any influence the presence of sodium ions may have upon decay is in progress. See SI section 5 for fitting details and assorted additional spectra.

SQUID Magnetometry. Temperature-dependent magnetic susceptibility measurements were carried out with a Quantum-Design MPMS-XL-5 SQUID magnetometer equipped with a 5 T magnet in the range from 2 to 295 K at a magnetic field of 0.5 T. The powdered sample was contained in a gel bucket and fixed in a nonmagnetic sample holder. Each raw data file for the measured magnetic moment was corrected for the diamagnetic contribution of the sample holder and the gel bucket. The molar susceptibility data were corrected for the diamagnetic contribution. Samples of **2** were prepared inside a glovebox under a nitrogen atmosphere with <0.1 ppm of O_2 and H_2O from crystalline material stored at −30 °C.

■ ASSOCIATED CONTENT

Ⓢ Supporting Information

Supplemental figures described in the text, detailed synthetic protocols and characterization data for compounds, experimental traces for O_2 uptake, crystallographic details for **2**, vibrational and UV−vis spectra, binding constant determination and magnetic measurement details, and substrate reactivity procedure and NMR spectrum. This material is available free of charge via the Internet at http://pubs.acs.org.

■ AUTHOR INFORMATION

Corresponding Author

*E-mail: Franc.Meyer@chemie.uni-goettingen.de.

Notes

The authors declare no competing financial interest.

■ ACKNOWLEDGMENTS

Financial support was provided by the Deutsche Forschungsgemeinschaft (IRTG 1422 Metal Sites in Biomolecules: Structures, Regulation and Mechanisms; see www.biometals.eu; PhD scholarship for K.D.) and T.G. was supported by the Volkswagen Stiftung via the Niedersachsenprofessur awarded to Prof. em. G. M. Sheldrick. This work was carried out in the framework of the European COST program CM1003.

■ REFERENCES

(1) Rolff, M.; Schottenheim, J.; Decker, H.; Tuczek, F. *Chem. Soc. Rev.* **2011**, *40*, 4077−4098.
(2) Itoh, S.; Fukuzumi, S. *Acc. Chem. Res.* **2007**, *40*, 592−600.
(3) Que, L.; Tolman, W. B. *Nature* **2008**, *455*, 333−340.
(4) Kitajima, N.; Fujisawa, K.; Morooka, Y.; Toriumi, K. *J. Am. Chem. Soc.* **1989**, *111*, 8975−8976.
(5) Solomon, E. I.; Ginsbach, J. W.; Heppner, D. E.; Kieber-Emmons, M. T.; Kjaergaard, C. H.; Smeets, P. J.; Tian, L.; Woertink, J. S. *Faraday Discuss.* **2011**, *148*, 11−39.
(6) Mirica, L. M.; Ottenwaelder, X.; Stack, T. D. P. *Chem. Rev.* **2004**, *104*, 1013−1045.
(7) Lewis, E. A.; Tolman, W. B. *Chem. Rev.* **2004**, *104*, 1047−1076.
(8) Himes, R. A.; Karlin, K. D. *Curr. Opin. Chem. Biol.* **2009**, *13*, 119−131.
(9) Reim, J.; Krebs, B. *Angew. Chem., Int. Ed.* **1994**, *33*, 1969−1971.
(10) Jacobson, R. R.; Tyeklar, Z.; Farooq, A.; Karlin, K. D.; Liu, S.; Zubieta, J. *J. Am. Chem. Soc.* **1988**, *110*, 3690−3692.
(11) Metz, M.; Solomon, E. I. *J. Am. Chem. Soc.* **2001**, *123*, 4938−4950.
(12) Tinberg, C. E.; Lippard, S. J. *Acc. Chem. Res.* **2011**, *44*, 280−288.
(13) Chachiyo, T.; Rodriguez, J. H. *Dalton Trans.* **2012**, *41*, 995−1003.
(14) Ross, P. K.; Solomon, E. I. *J. Am. Chem. Soc.* **1991**, *113*, 3246−3259.
(15) Baldwin, M. J.; Root, D. E.; Pate, J. E.; Fujisawa, K.; Kitajima, N.; Solomon, E. I. *J. Am. Chem. Soc.* **1992**, *114*, 10421−10431.
(16) Baldwin, M. J.; Ross, P. K.; Pate, J. E.; Tyeklar, Z.; Karlin, K. D.; Solomon, E. I. *J. Am. Chem. Soc.* **1991**, *113*, 8671−8679.
(17) Schenker, R.; Kieber-Emmons, M. T.; Riordan, C. G.; Brunold, T. C. *Inorg. Chem.* **2005**, *44*, 1752−1762.
(18) Meyer, F.; Pritzkow, H. *Angew. Chem., Int. Ed.* **2000**, *39*, 2112−2115.
(19) Buchler, S.; Meyer, F.; Kaifer, E.; Pritzkow, H. *Inorg. Chim. Acta* **2002**, *337*, 371−386.
(20) Klingele, J.; Dechert, S.; Meyer, F. *Coord. Chem. Rev.* **2009**, *253*, 2698−2741.
(21) Kubas, G. J.; Monzyk, B.; Crumbliss, A. L. *Inorg. Synth.* **1990**, *28*, 68−70.
(22) Würtele, C.; Heinemann, F. W.; Schindler, S. *J. Coord. Chem.* **2010**, *63*, 2629−2641.
(23) Garcia-Bosch, I.; Company, A.; Frisch, J. R.; Torrent-Sucarrat, M.; Cardellach, M.; Gamba, I.; Güell, M.; Casella, L.; Que, L.; Ribas, X.; Luis, J. M.; Costas, M. *Angew. Chem., Int. Ed.* **2010**, *49*, 2406−2409.
(24) Lucas, H. R.; Li, L.; Sarjeant, A. a N.; Vance, M. a; Solomon, E. I.; Karlin, K. D. *J. Am. Chem. Soc.* **2009**, *131*, 3230−3245.
(25) Comba, P.; Haaf, C.; Helmle, S.; Karlin, K. D.; Pandian, S.; Waleska, A. *Inorg. Chem.* **2012**, *51*, 2841−2851.
(26) Würtele, C.; Sander, O.; Lutz, V.; Waitz, T.; Tuczek, F.; Schindler, S. *J. Am. Chem. Soc.* **2009**, *131*, 7544−7545.
(27) Sheldrick, G. M. *Acta Crystallogr., Sect. A* **2008**, *64*, 112−122.
(28) STOE & CIE Gmbh. X-RED, 2002.
(29) Gabadinho, J.; Beteva, A.; Guijarro, M.; Rey-Bakaikoa, V.; Spruce, D.; Bowler, M. W.; Brockhauser, S.; Flot, D.; Gordon, E. J.; Hall, D. R.; Lavault, B.; McCarthy, A. A.; McCarthy, J.; Mitchell, E.; Monaco, S.; Mueller-Dieckmann, C.; Nurizzo, D.; Ravelli, R. B. G.; Thibault, X.; Walsh, M. A.; Leonard, G. A.; McSweeney, S. M. *J. Synchrotron Radiat.* **2010**, *17*, 700−707.
(30) Kabsch, W. *Acta Crystallogr., Sect. D: Biol. Crystallogr.* **2010**, *66*, 125−132.
(31) Emsley, P.; Lohkamp, B.; Scott, W. G.; Cowtan, K. *Acta Crystallogr., Sect. D: Biol. Crystallogr.* **2010**, *66*, 486−501.
(32) Hübschle, C. B.; Sheldrick, G. M.; Dittrich, B. *J. Appl. Crystallogr.* **2011**, *44*, 1281−1284.
(33) Komiyama, K.; Furutachi, H.; Nagatomo, S.; Hashimoto, A.; Hayashi, H.; Fujinami, S.; Suzuki, M.; Kitagawa, T. *Bull. Chem. Soc. Jpn.* **2004**, *77*, 59−72.
(34) Weitzer, M.; Schindler, S.; Brehm, G.; Schneider, S.; Hörmann, E.; Jung, B.; Kaderli, S.; Zuberbühler, A. D. *Inorg. Chem.* **2003**, *42*, 1800−1806.
(35) Hoppe, T.; Schaub, S.; Becker, J.; Würtele, C.; Schindler, S. *Angew. Chem., Int. Ed.* **2013**, *52*, 870−873.
(36) The τ parameter describes the trigonality of a five coordinate structure. Thus, for an ideal trigonal bipyramid $\tau = 1$, whereas a value of $\tau = 0$ indicates perfect square pyramidal geometry. See: Addison, A. W.; Rao, T. N.; Reedijk, J.; van Rijn, J.; Verschoor, G. C. *J. Chem. Soc., Dalton Trans.* **1984**, 1349−1356.
(37) Gražulis, S.; Chateigner, D.; Downs, R. T.; Yokochi, a F. T.; Quirós, M.; Lutterotti, L.; Manakova, E.; Butkus, J.; Moeck, P.; Le Bail, A. *J. Appl. Crystallogr.* **2009**, *42*, 726−729.
(38) Liu, Q.-X.; Zhou, Z.-H. *Polyhedron* **2012**, *35*, 1−6.
(39) Uhl, W.; Halvagar, M. R.; Rogel, F.; Massa, W. *Eur. J. Inorg. Chem.* **2009**, *2009*, 489−492.
(40) Grzywa, M.; Nitek, W.; Łasocha, W. *J. Mol. Struct.* **2008**, *888*, 318−326.
(41) Runde, W.; Brodnax, L. F.; Goff, G. S.; Peper, S. M.; Taw, F. L.; Scott, B. L. *Chem. Commun.* **2007**, *2*, 1728−1729.
(42) Skulan, A. J.; Hanson, M. A.; Hsu, H.; Que, L.; Solomon, E. I. *J. Am. Chem. Soc.* **2003**, *125*, 7344−7356.

(43) Peterson, R. L.; Himes, R. A.; Kotani, H.; Suenobu, T.; Tian, L.; Siegler, M. A.; Solomon, E. I.; Fukuzumi, S.; Karlin, K. D. *J. Am. Chem. Soc.* **2011**, *133*, 1702−1705.
(44) Park, J.; Morimoto, Y.; Lee, Y.-M.; You, Y.; Nam, W.; Fukuzumi, S. *Inorg. Chem.* **2011**, *50*, 11612−11622.
(45) Park, J.; Morimoto, Y.; Lee, Y.; Nam, W.; Fukuzumi, S. *J. Am. Chem. Soc.* **2011**, *133*, 5236−5239.
(46) Chen, J.; Lee, Y.-M.; Davis, K. M.; Wu, X.; Seo, M. S.; Cho, K.-B.; Yoon, H.; Park, Y. J.; Fukuzumi, S.; Pushkar, Y. N.; Nam, W. *J. Am. Chem. Soc.* **2013**, *135*, 6388−6391.
(47) Fukuzumi, S.; Morimoto, Y.; Kotani, H.; Naumov, P.; Lee, Y.-M.; Nam, W. *Nat. Chem.* **2010**, *2*, 756−759.
(48) Leeladee, P.; Baglia, R. A.; Prokop, K. A.; Latifi, R.; de Visser, S. P.; Goldberg, D. P. *J. Am. Chem. Soc.* **2012**, *134*, 10397−10400.
(49) Morimoto, Y.; Kotani, H.; Park, J.; Lee, Y.-M.; Nam, W.; Fukuzumi, S. *J. Am. Chem. Soc.* **2011**, *133*, 403−405.
(50) Lee, Y.-M.; Bang, S.; Kim, Y. M.; Cho, J.; Hong, S.; Nomura, T.; Ogura, T.; Troeppner, O.; Ivanović-Burmazović, I.; Sarangi, R.; Fukuzumi, S.; Nam, W. *Chem. Sci.* **2013**, *4*, 3917−3923.
(51) Badiei, Y.; Warren, T. H.; Chiang, K. P.; Holland, P. L. *Inorg. Synth.* **2010**, *35*, 50−53.
(52) Thordarson, P. *Chem. Soc. Rev.* **2011**, *40*, 1305−1323.
(53) Karlin, K. D.; Tyeklár, Z.; Farooq, A.; Jacobson, R. R.; Sinn, E.; Lee, D. W.; Bradshaw, J. E.; Wilson, L. J. *Inorg. Chim. Acta* **1991**, *182*, 1−3.
(54) Solomon, E. I.; Dooley, D. M.; Wang, R.-H.; Gray, H. B.; Cerdonio, M.; Mogno, F.; Romani, G. L. *J. Am. Chem. Soc.* **1976**, *98*, 1029−1031.
(55) Prokofieva, A.; Prikhod'ko, A. I.; Enyedy, E. A.; Farkas, E.; Maringgele, W.; Demeshko, S.; Dechert, S.; Meyer, F. *Inorg. Chem.* **2007**, *46*, 4298−4307.
(56) Driessen, W. L.; Chang, L.; Finazzo, C.; Gorter, S.; Rehorst, D.; Reedijk, J.; Lutz, M.; Spek, A. L. *Inorg. Chim. Acta* **2003**, *350*, 25−31.
(57) Iskander, M. F.; Khalil, T. E.; Haase, W.; Werner, R.; Svoboda, I.; Fuess, H. *Polyhedron* **2001**, *20*, 2787−2798.
(58) Frensch, L. K.; Pröpper, K.; John, M.; Demeshko, S.; Brückner, C.; Meyer, F. *Angew. Chem., Int. Ed.* **2011**, *50*, 1420−1424.
(59) Blusch, L. K.; Craigo, K. E.; Martin-Diaconescu, V.; McQuarters, A. B.; Bill, E.; Dechert, S.; DeBeer, S.; Lehnert, N.; Meyer, F. *J. Am. Chem. Soc.* **2013**, *135*, 13892−13899.
(60) Leibeling, G.; Demeshko, S.; Dechert, S.; Meyer, F. *Angew. Chem., Int. Ed.* **2005**, *44*, 7111−7114.
(61) Shaik, S.; Chen, H.; Janardanan, D. *Nat. Chem.* **2011**, *3*, 19−27.
(62) Comba, P.; Martin, B.; Muruganantham, A.; Straub, J. *Inorg. Chem.* **2012**, *51*, 9214−9225.
(63) Meyer, F.; Heinze, K.; Nuber, B.; Zsolnai, L. *J. Chem. Soc., Dalton Trans.* **1998**, 207−213.
(64) Ackermann, J.; Meyer, F.; Kaifer, E.; Pritzkow, H. *Chem. Eur. J.* **2002**, *8*, 247−258.